INTERNATIONAL JOURNAL FOR NUMERICAL METHODS IN FLUIDS
Int. J. Numer. Meth. Fluids 2008; **58**:287–306
Published online 17 March 2008 in Wiley InterScience (www.interscience.wiley.com). DOI: 10.1002/fld.1708

Spectral/*hp* penalty least-squares finite element formulation for unsteady incompressible flows

V. Prabhakar*, † and J. N. Reddy

Department of Mechanical Engineering, Texas A&M University, College Station, TX 77843, U.S.A.

SUMMARY

In this paper, we present spectral/*hp* penalty least-squares finite element formulation for the numerical solution of unsteady incompressible Navier–Stokes equations. Pressure is eliminated from Navier–Stokes equations using penalty method, and finite element model is developed in terms of velocity, vorticity and dilatation. High-order element expansions are used to construct discrete form. Unlike other penalty finite element formulations, equal-order Gauss integration is used for both viscous and penalty terms of the coefficient matrix. For time integration, space–time decoupled schemes are implemented. Second-order accuracy of the time integration scheme is established using the method of manufactured solution. Numerical results are presented for impulsively started lid-driven cavity flow at Reynolds number of 5000 and transient flow over a backward-facing step. The effect of penalty parameter on the accuracy is investigated thoroughly in this paper and results are presented for a range of penalty parameter. Present formulation produces very accurate results for even very low penalty parameters (10–50). Copyright © 2008 John Wiley & Sons, Ltd.

Received 13 November 2006; Revised 1 November 2007; Accepted 6 November 2007

KEY WORDS: penalty method; spectral/*hp* method; least-squares method; viscous incompressible flow

1. INTRODUCTION

In the past few years, finite element models based on least-squares functionals have drawn considerable attention [1–7]. Given a set of partial differential equations, the least-squares method allows us to define an unconstrained minimization problem. These formulations have several advantages over the traditionally used weak-form Galerkin formulations. Most notably, the least-squares

*Correspondence to: V. Prabhakar, Department of Mechanical Engineering, Texas A&M University, College Station, TX 77843, U.S.A.
†E-mail: prabhakarv@tamu.edu, vivek.prabhakar@halliburton.com

Contract/grant sponsor: Air Force Office of Scientific Research; contract/grant number: F49620-03-1-0201
Contract/grant sponsor: Army Research Office; contract/grant number: 45508-EG

Copyright © 2008 John Wiley & Sons, Ltd.

formulations circumvent the inf–sup condition of Ladyzhenskaya–Babuska–Brezzi (LBB). Hence, the choice of approximating space is not subject to LBB conditions. Also, the resulting algebraic system is symmetric and positive definite.

Previous study of Pontaza and Reddy [4] showed that in these formulations, temporal evolution of pressure field ill-behaves, which in turn leads to spurious solutions in many cases. Unsteady problems, especially with inflow/outflow boundaries, produce spurious pressure evolution with time, mainly due to the lack of strong pressure velocity coupling. In these formulations, the divergence-free constraint on the velocity field is enforced directly through the least-squares functional, and pressure does not play a role in enforcing divergence-free constraint.

Recently, Prabhakar and Reddy [6] presented a spectral/*hp* penalty least-squares finite element formulation for steady incompressible Navier–Stokes equations. For steady-state flows, pressure evolution does not pose any problem. In this study, we extend this formulation to unsteady problems. For time integration, space–time decoupled formulations are popular, where discretization in space and time is carried out separately. In space–time decoupled formulations, least-squares variational principles are applied in space only. Pontaza and Reddy [4] and Bell and Surana [8] implemented space–time coupled least-squares formulations. These formulations have higher accuracy than decoupled formulations, but associated computational costs are very high. A two-dimensional problem becomes a three-dimensional problem, with time as the additional dimension. In this study, we implement space–time decoupled time integration schemes, namely Crank–Nicholson scheme and backward multi-step scheme (BDF2).

In another study, Prabhakar *et al.* [9] extended this idea for unsteady problems and implemented it using low-order basis functions (bilinear) with one-point Gauss quadrature, which is equivalent to the collocation approach. The p-version of the finite element method is known to possess superior convergence characteristics compared with the h-version. Nevertheless, most of the current finite element research has involved the use of low-order approximations, mainly because of low computational cost associated with the h-version. If high accuracy is required, then we may justify using high-order methods by the fact that the error will converge at a faster rate than the operation count increases. Therefore, it will ultimately be more efficient to use high-order methods. Nevertheless, the cross-over point between required accuracy and relative computational cost of low- and high-order methods for a given application is a point of much debate.

Several studies have been reported on penalty models implemented in the context of weak-form Galerkin formulation. They achieved some popularity, mainly because they circumvent LBB stability condition. Also there is a reduction in the number of independent variables. Almost all these studies use low-order basis functions and reduced-order integration for penalty terms to circumvent locking. Also, the penalty parameter used is of the order 10^8–10^{12}. For such a penalty parameter, the coefficient matrix is ill conditioned and iterative solvers do not perform well. In this study, high-order element expansions are used to construct the discrete model, which does not experience locking. Equal-order integration is used for all the terms of the coefficient matrix.

This paper is organized as follows. In Section 2, the penalty least-squares finite element model for incompressible Navier–Stokes equations is presented. Numerical results are presented in Section 3. First, the second-order accuracy of the time integration scheme is established using the method of manufactured solution. Next, we present results for two-dimensional impulsively started lid-driven cavity at Reynolds number of 5000. Lastly, numerical results are presented for the transient two-dimensional flow over a backward-facing step. Simulations for various penalty parameters are carried out, and evolutions of velocity and pressure fields with time are reported.

Copyright © 2008 John Wiley & Sons, Ltd.

DOI: 10.1002/fld

2. PENALTY FORMULATION FOR INCOMPRESSIBLE NAVIER–STOKES EQUATIONS

In the penalty method, the continuity equation is treated as a constraint, which is included back into the formulation in a least-squares sense. This amounts to replacing pressure in Navier–Stokes equations with the following expression (see [10–12] for additional details):

$$p = -\gamma(\nabla \cdot \mathbf{u}) \tag{1}$$

Gunzburger [13] proposed an iterative penalty method in which the pressure is updated using the formula

$$p^n = p^{n-1} - \gamma(\nabla \cdot \mathbf{u}) \tag{2}$$

2.1. The velocity–dilatation–vorticity first-order system

In the interest of reducing the order of the equations to avoid C^k-approximation ($k \geqslant 1$) of the field variables, we cast the second-order Navier–Stokes equations as a set of first-order equations by introducing the vorticity vector, $\boldsymbol{\omega} = \nabla \times \mathbf{u}$, and dilatation, $D = \nabla \cdot \mathbf{u}$, as independent dependent variables. Then, the problem can be stated as one of finding the velocity vector $\mathbf{u}(\mathbf{x})$, dilatation $D(\mathbf{x})$ and vorticity $\boldsymbol{\omega}(\mathbf{x})$ such that

$$\frac{\partial \mathbf{u}}{\partial t} + (\mathbf{u} \cdot \nabla)\mathbf{u} - \gamma \nabla D + \frac{1}{Re} \nabla \times \boldsymbol{\omega} = \mathbf{f} - \nabla p^{n-1} \quad \text{in } \Omega \times (0, \tau] \tag{3}$$

$$\boldsymbol{\omega} - \nabla \times \mathbf{u} = \mathbf{0} \quad \text{in } \Omega \times (0, \tau] \tag{4}$$

$$D - \nabla \cdot \mathbf{u} = 0 \quad \text{in } \Omega \times (0, \tau] \tag{5}$$

$$\mathbf{u} = \mathbf{u}_0(\mathbf{x}) \quad \text{on } \Gamma_u \tag{6}$$

$$\mathbf{u} = \mathbf{u}^s \quad \text{on } \Gamma_u \times (0, \tau] \tag{7}$$

$$\boldsymbol{\omega} = \boldsymbol{\omega}^s \quad \text{on } \Gamma_\omega \times (0, \tau] \tag{8}$$

Typically, $\Gamma_u \cap \Gamma_\omega = \emptyset$, i.e. if velocity is specified at a boundary, vorticity need not be specified there.

2.1.1. L_2 least-squares formulation. The least-squares functional of the problem can be set up by summing up the squares of the residuals of the new set of equations. For time integration, space–time decoupled formulations are used. In space–time decoupled formulations, discretizations in space and time are introduced independently. Generally, the temporal operators are represented by truncated Taylor series expansions in time domain. We use Crank–Nicholson or backward multi-step scheme (BDF2). Least-squares functional for backward multi-step schemes can be expressed as

$$\mathscr{J}(\mathbf{u}, D, \boldsymbol{\omega}; \mathbf{f}) = \frac{1}{2}\left(\left\| \frac{\gamma_0}{\Delta t}\mathbf{u}^{s+1} - \sum_{q=0}^{M_\alpha} \frac{\beta_q}{\Delta t}\mathbf{u}^{s-q} + (\mathbf{u} \cdot \nabla)\mathbf{u} - \gamma \nabla D + \frac{1}{Re}\nabla \times \boldsymbol{\omega} - \mathbf{f} + \nabla p^{n-1} \right\|^2_{0,\Omega\times(0,\tau]} + \|\boldsymbol{\omega} - \nabla \times \mathbf{u}\|^2_{0,\Omega\times(0,\tau]} + \|D - \nabla \cdot \mathbf{u}\|^2_{0,\Omega\times(0,\tau]} \right) \tag{9}$$

Copyright © 2008 John Wiley & Sons, Ltd.

DOI: 10.1002/fld

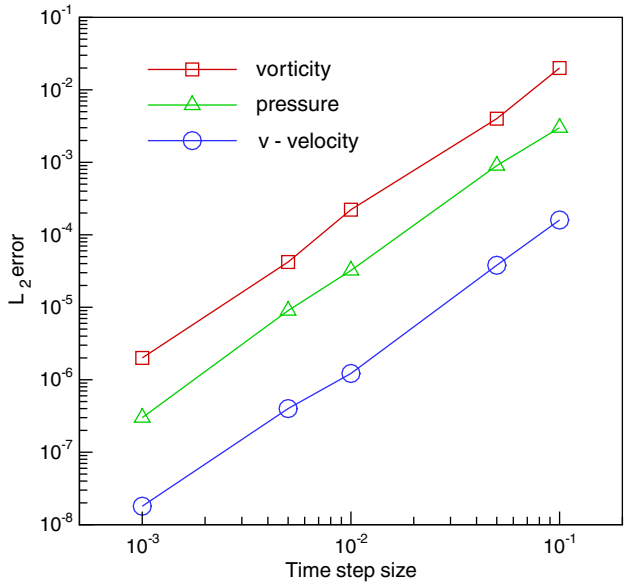

Figure 1. Convergence of velocity, pressure and vorticity fields in the L_2-norm for decreasing time step size.

where $\gamma_0 = \sum_{q=0}^{M_\alpha} \beta_q$ for consistency, β_q are weights associated with a particular multi-step scheme and $\Delta t = t_{s+1} - t_s$ is the time increment.

Considering the homogeneous, pure velocity, boundary condition case, the least-squares principle for functional (9) can be stated as follows:

find $(\mathbf{u}, D, \boldsymbol{\omega}) \in \mathbf{X}, \mathbf{u}(\mathbf{x}, 0) = \mathbf{u}_0(\mathbf{x})$ such that

$$\mathscr{J}(\mathbf{u}, D, \boldsymbol{\omega}; \mathbf{f}) \leqslant \mathscr{J}(\tilde{\mathbf{u}}, \tilde{D}, \tilde{\boldsymbol{\omega}}; \mathbf{f}) \quad \forall (\tilde{\mathbf{u}}, \tilde{D}, \tilde{\boldsymbol{\omega}}) \in \mathbf{X} \tag{10}$$

where we use the space

$$\mathbf{X} = \{(\mathbf{u}, D, \boldsymbol{\omega}) \in \mathbf{H}_0^1(\Omega) \times H^1(\Omega) \times \mathbf{H}^1(\Omega)\}$$

For detailed formulation, see [6, 9].

2.1.2. Expansion bases. Nodal expansion: In the standard interval $\Omega_{\text{st}} = \{\xi | -1 < \xi < 1\}$, nodal expansions are defined as

$$\psi_i(\xi) = \frac{(\xi - 1)(\xi + 1) L_p'(\xi)}{p(p+1) L_p(\xi_i)(\xi - \xi_i)} \tag{11}$$

In Equation (11), $L_p = P_p^{0,0}$ is the Legendre polynomial of order p, and ξ_i denotes the location of the roots of $(\xi - 1)(\xi + 1) L_p'(\xi) = 0$ in the interval $[-1, 1]$. Details on the multidimensional construction of nodal expansions can be found in Reference [14]. The integrals are evaluated using Gauss–Lobatto–Legendre quadrature rule. For details on standard finite element computer

Copyright © 2008 John Wiley & Sons, Ltd.

DOI: 10.1002/fld

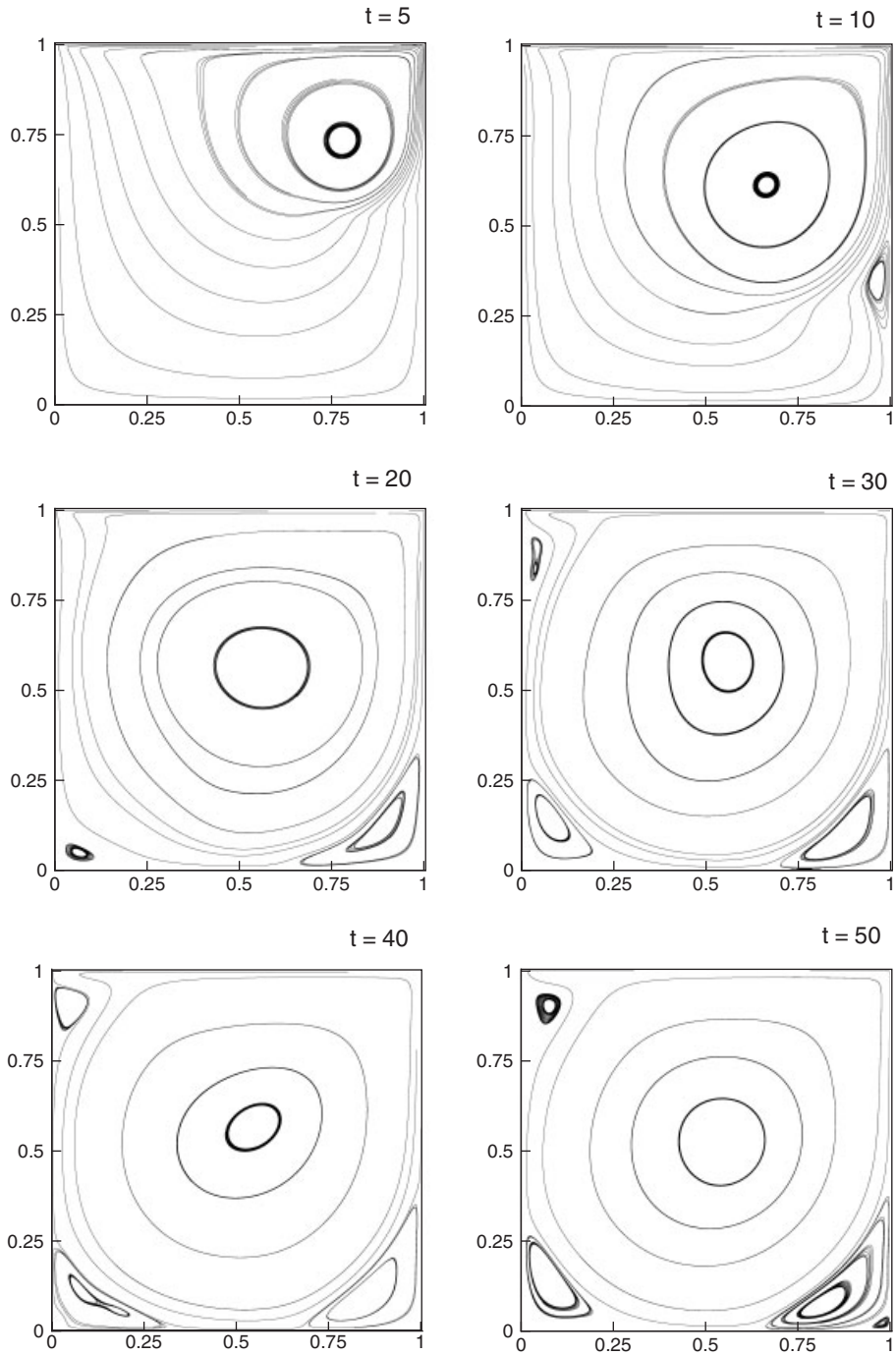

Figure 2. Time history of streamline plots for impulsively started lid-driven cavity flow at $Re = 5000$.

Copyright © 2008 John Wiley & Sons, Ltd.

DOI: 10.1002/fld

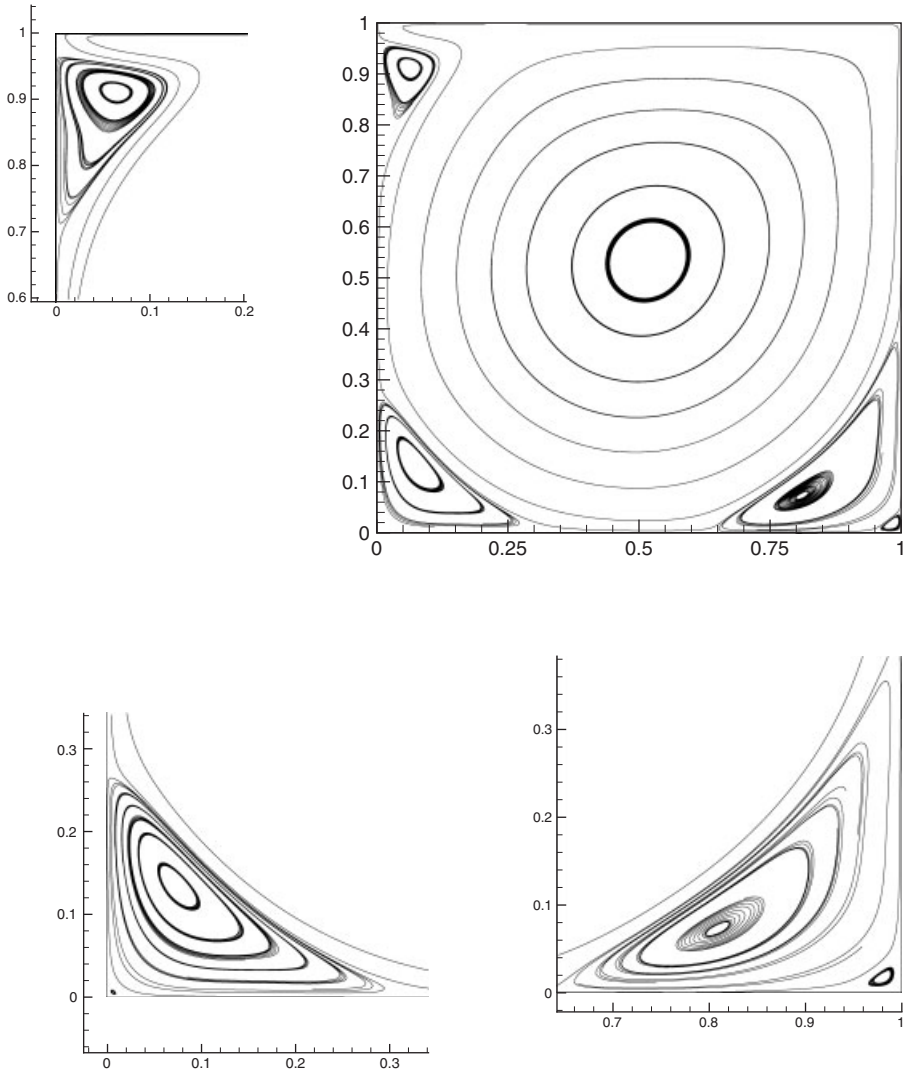

Figure 3. Streamlines at steady state for lid-driven cavity flow.

implementation, such as mapping $\bar{\Omega}_e \rightleftarrows \hat{\Omega}_e$, numerical integration in $\hat{\Omega}_e$ and assembly using the direct stiffness approach, see Reddy [10, 11]. For linearization, we use Newton's method, details of which can be found in [8].

3. NUMERICAL RESULTS

In this section, numerical results obtained with the present least-squares finite element model are presented. First, second-order accuracy of the time integration scheme used is verified. Next,

Copyright © 2008 John Wiley & Sons, Ltd.

DOI: 10.1002/fld

Table I. Location of vortices: comparison with the benchmark results of Ghia.

	Present	Ghia *et al.* [16]
Primary	0.5147, 0.5341	0.5117, 0.5352
First BR	0.8085, 0.0725	0.8086, 0.0742
First BL	0.0743, 0.1347	0.0703, 0.1367
First TL	0.0640, 0.9107	0.0625, 0.9102
Second BR	0.9801, 0.0166	0.9805, 0.0195
Second BL	0.0073, 0.0074	0.0117, 0.0078

results are presented for impulsively started lid-driven cavity problem and transient flow over a backward-facing step problem.

For all the problems considered in this section, non-linear convergence is declared when the relative norm of the residual, $\|\Delta\mathbf{U}\|/\|\mathbf{U}\|$, is less than 10^{-3}, unless mentioned otherwise, where $\mathbf{U}$ is the solution vector (includes all degrees of freedom at a node). Convergence of the conjugate gradient method to solve the equations is declared when the L_2-norm of error is less than 10^{-6}.

3.1. Verification problem

In the first numerical example, we establish the second-order accuracy of the time integration scheme used. We use the method of manufactured solutions [15]. We consider a unit square and take the exact solution of the incompressible Navier–Stokes equations to be of the form:

$$u(x,y,t)=\pi\sin^2(\pi x)\sin(\pi y)\cos(\pi y)\sin(t)$$

$$v(x,y,t)=-\pi\sin(\pi x)\cos(\pi x)\sin^2(\pi y)\sin(t)$$

$$p(x,y,t)=\cos(\pi x)\sin(\pi y)\sin(t)$$

The prescribed velocity field satisfies continuity equation, and the source term $\mathbf{f}$ of the momentum equations represents the residual of the differential equations such that the prescribed solution is the exact solution to the problem.

The Dirichlet boundary conditions on velocities are specified using the exact solution given above. The discrete system is linearized using Newton's method, and the resulting symmetric positive-definite (SPD) system of equations has been solved using the Choleski factorization. A 4×4 uniform mesh of quadrilateral elements is used for spatial discretization. Newton's convergence is declared when the relative norm of the residual is less than 10^{-10}. The penalty parameter used is 10^2 for which L_2-norm of the residual of continuity equation is below 10^{-12} and does not interfere with the convergence. For time discretization, BDF2 scheme is used.

The time evolution of fields is computed for $t\in[0,20]$ for decreasing time step size varying from 10^{-1} to 10^{-3}. The L_2 error in v-velocity, pressure and vorticity is recorded at $t=5$ and plotted in Figure 1 as a function of time step on log–log scale. The errors decay at an algebraic rate with slope 2, as expected for the second-order accurate time integration scheme.

3.2. Two-dimensional lid-driven cavity flow

Next, the two-dimensional lid-driven cavity problem is analyzed to test the presented formulation. The flow is driven by the translation of the top boundary. No slip boundary condition is imposed on

Copyright © 2008 John Wiley & Sons, Ltd.

DOI: 10.1002/fld

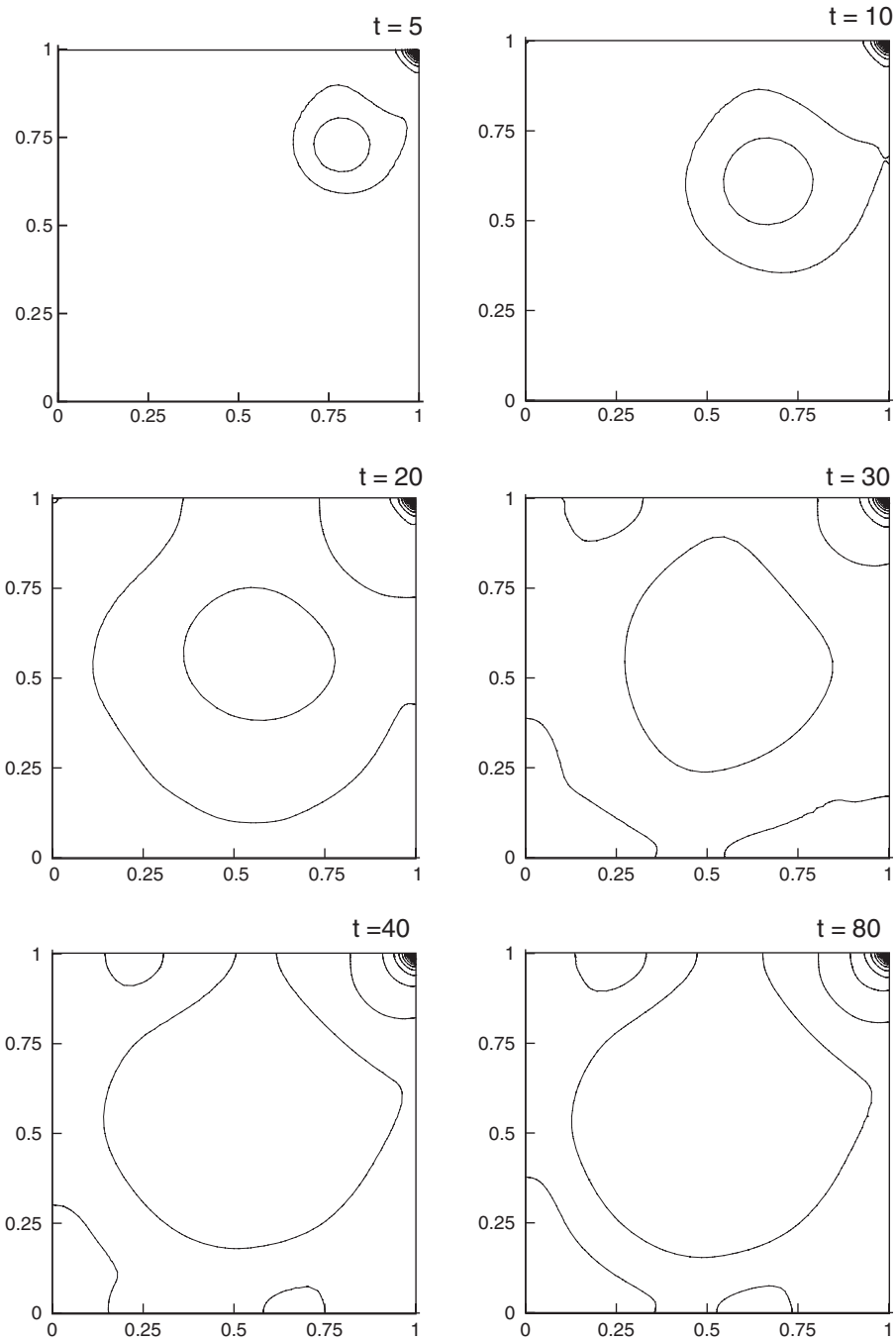

Figure 4. Time history of pressure contours for impulsively started lid-driven cavity flow.

Copyright © 2008 John Wiley & Sons, Ltd.

DOI: 10.1002/fld

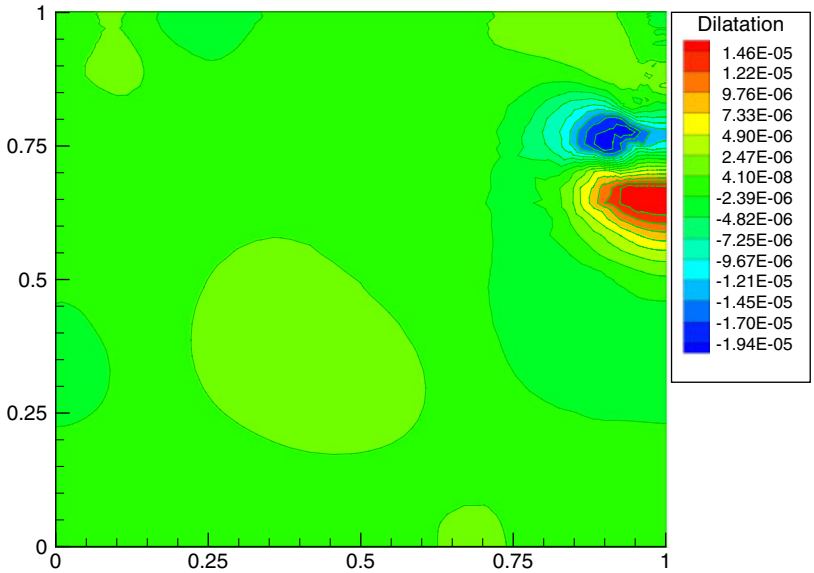

Figure 5. Dilatation contours for lid-driven cavity at time = 100.

all solid walls. On the top wall ($y=1.0$), the boundary conditions are taken as $u=\hat{u}(x,t)$, $v=0$. To avoid singularity in the boundary condition, we specify a hyperbolic tangent u-velocity distribution on the top wall:

$$u_{\text{lid}}(x)=\begin{cases}\tanh(\beta x) & 0\leqslant x\leqslant 0.5\\ -\tanh(\beta(x-1)) & 0.5<x\leqslant 1.0\end{cases}$$

with $\beta>0$. In this study, $\beta=50$ is used, which gives a smooth but at the same time sharp transition from $u=0.0$ to 1.0 near the walls of the driven surface. This boundary condition results in a well-posed boundary condition as singularities at the corners are eliminated. The standard boundary condition ($u=1$ everywhere) would make the problem singular and destroys the high-accuracy properties associated with high-order expansions by polluting the solution near the corners. High-order methods are sensitive to these types of singularities.

The u-velocity of the driven surface also varies in time according to a hyperbolic tangent distribution. Hence, lid velocity is given by $\hat{u}(x,t)=u_{\text{lid}}(x)\tanh(t)$.

We use 14×14 nonuniform mesh that is graded towards the wall; the corner elements have a dimension of 0.01×0.01. The seventh-order nodal expansion is used in each element, and there are a total of 39 204 degrees of freedom in the mesh. All internal degrees of freedom are condensed out using Schur complement method (see [6] for details), resulting in 10 980 interface degrees of freedom with a bandwidth of 788. The preconditioned conjugate gradient is used to solve for the interface degrees of freedom. This problem has been solved for the penalty parameters 10 and 30. Reynolds number is taken to be 5000. Initial velocity conditions are taken to be zero everywhere. The Crank–Nicholson scheme is used for time marching, and a time increment of 0.2 has been used for all results reported in this section.

Copyright © 2008 John Wiley & Sons, Ltd.

DOI: 10.1002/fld

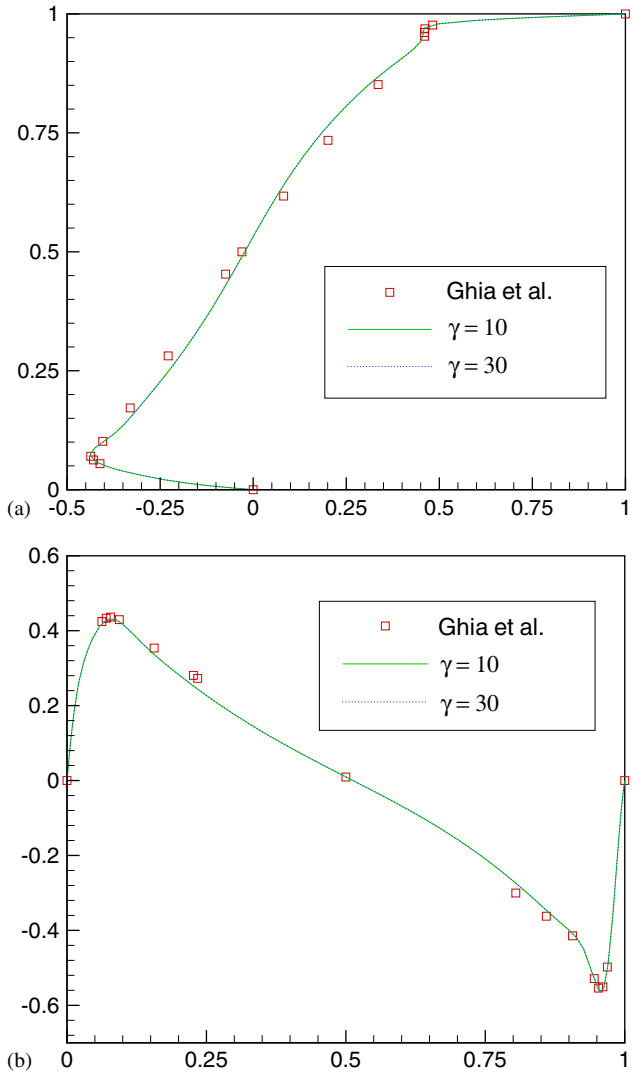

Figure 6. (a) Steady-state u-velocity profile along the vertical middle line of the cavity and (b) steady-state v-velocity profile along the horizontal middle line of the cavity: comparison with Ghia *et al.* [16].

Figure 2 contains streamline plots for various times. Upon start-up, a long narrow vortex forms close to the lid. The vortex gradually moves to the right and begins to grow.

Streamlines at steady state are shown in Figure 3. At steady state, there is one primary vortex, three first vortices, at the left and right bottom corners, named BR and BL, and the top left corner is named TL; two second vortices appear at the left and right bottom corners. Centers of these vortices are reported in Table I and compared with the benchmark values of Ghia *et al.* [16]. These values match well with the corresponding values of Ghia *et al.* [16]. A penalty parameter of 10 is used for these results. The value of the L_2 least-squares functional remains below 3.4×10^{-2} and

Copyright © 2008 John Wiley & Sons, Ltd.

DOI: 10.1002/fld

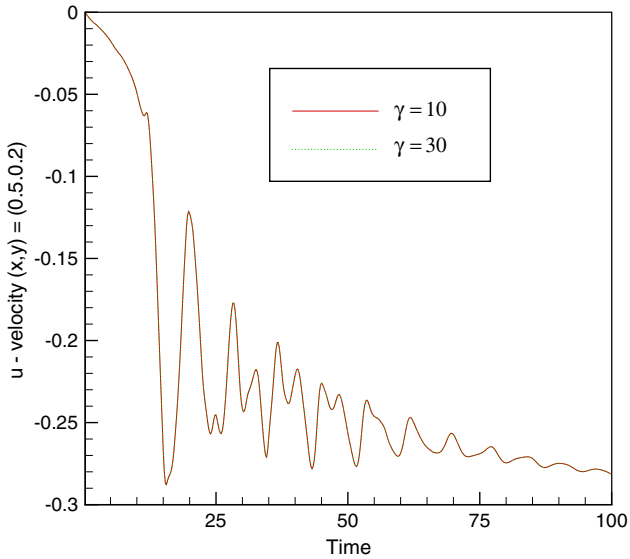

Figure 7. Time history of the u-velocity component.

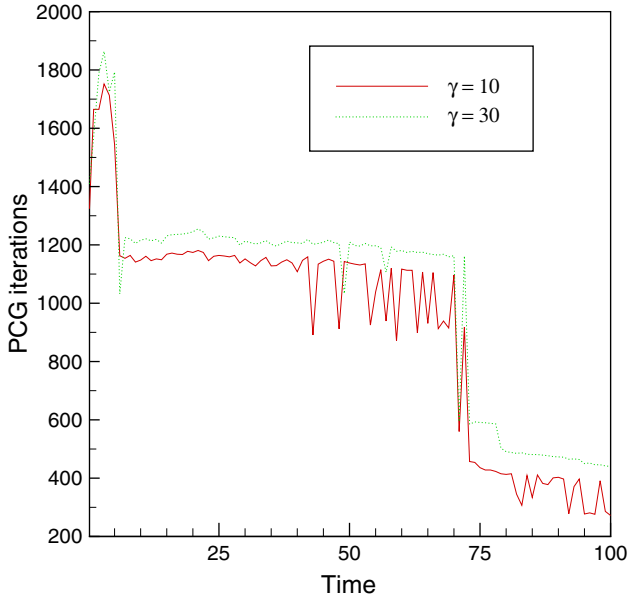

Figure 8. Time history of PCG iterations for impulsively started lid-driven cavity flow.

Copyright © 2008 John Wiley & Sons, Ltd.

DOI: 10.1002/fld

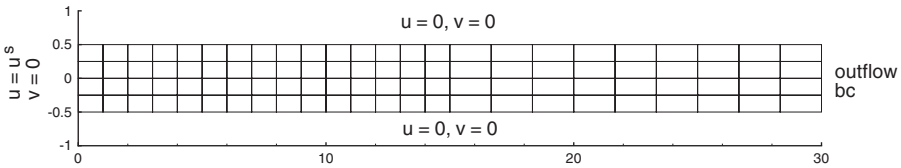

Figure 9. Geometry and boundary conditions for flow over a backward-facing step.

L_2-norm of the residual of continuity equation is below 10^{-5} at all times for the penalty parameter of 30. Typically, it takes two Newton's iterations to converge for every time step. Figure 4 shows pressure contours. Pressure $p=0$ is specified at the center of the cavity.

Dilatation contours are shown in Figure 5; it is clear that mass conservation is satisfied very well locally at all points in the domain, with a maximum value of dilatation approximately 1×10^{-5} near the top corner. The penalty parameter used in this case is only 10, and it works very well even for this high Reynolds number.

The u-velocity profiles along the vertical middle line of the cavity $x=0.5$ at steady state are shown in Figure 6(a) for various values of the penalty parameter, and the results are compared with those of Ghia *et al.* [16]. Again, we see good agreement between the two solutions even for $\gamma=10$.

In Figure 6(b), v-velocity profiles are plotted along the horizontal middle line of the cavity $y=0.5$ for various values of the penalty parameter. We note that boundary conditions are slightly different for the two studies. Ghia *et al.* [16] used lid velocity of 1.0 everywhere on the top wall, whereas in our case lid velocity varies with x and time. Also, Ghia *et al.* [16] used steady-state solver, whereas we use transient solver. This difference is the reason of a slight disagreement in the results.

Time history of u-velocity at $(0.5, 0.2)$ is plotted in Figure 7 for penalty parameters of 10 and 30. These penalty parameters give identical time evolution of the velocity field. Steady state is reached around $t=120$ nondimensional time.

Next, the number of PCG iterations required for the convergence of PCG solver is plotted against time in Figure 8 for penalty parameters of 10 and 30. Each data point in the plot represents the sum of PCG iterations at each Newton step, thus indicating the total number of PCG iterations required to converge at a time step.

As Figures 6(a) and (b) indicate, the present model gives very accurate results for even a penalty parameter of 10. Typical penalty parameter values used in the traditional penalty finite element model are in the range of 10^8–10^{12}. For such a high penalty parameter, conditioning number of the resulting coefficient matrix becomes very high, and different order integration rule is used to integrate penalty terms to obtain *acceptable* solution. In this study, we have used equal-order integration for all terms.

3.3. Transient flow over a backward-facing step

Next, we consider transient flow over a two-dimensional backward-facing step at $Re=800$. The domain of interest is $\bar{\Omega}=[0,30]\times[-0.5,0.5]$. Mesh and boundary conditions are shown in Figure 9. The boundary and initial conditions used here are the same as those used in the works of Gresho *et al.* [17] and Pontaza and Reddy [4]: $u=v=0$ on the horizontal walls, $-p+\mu\partial u/\partial n=0$ and $\partial v/\partial n=0$ on the outflow boundary and $u=[\tanh(t/4)]u_b(y)+[1-\tanh(t/4)]u_p(y)$ and $v=0$ on

Copyright © 2008 John Wiley & Sons, Ltd.

DOI: 10.1002/fld

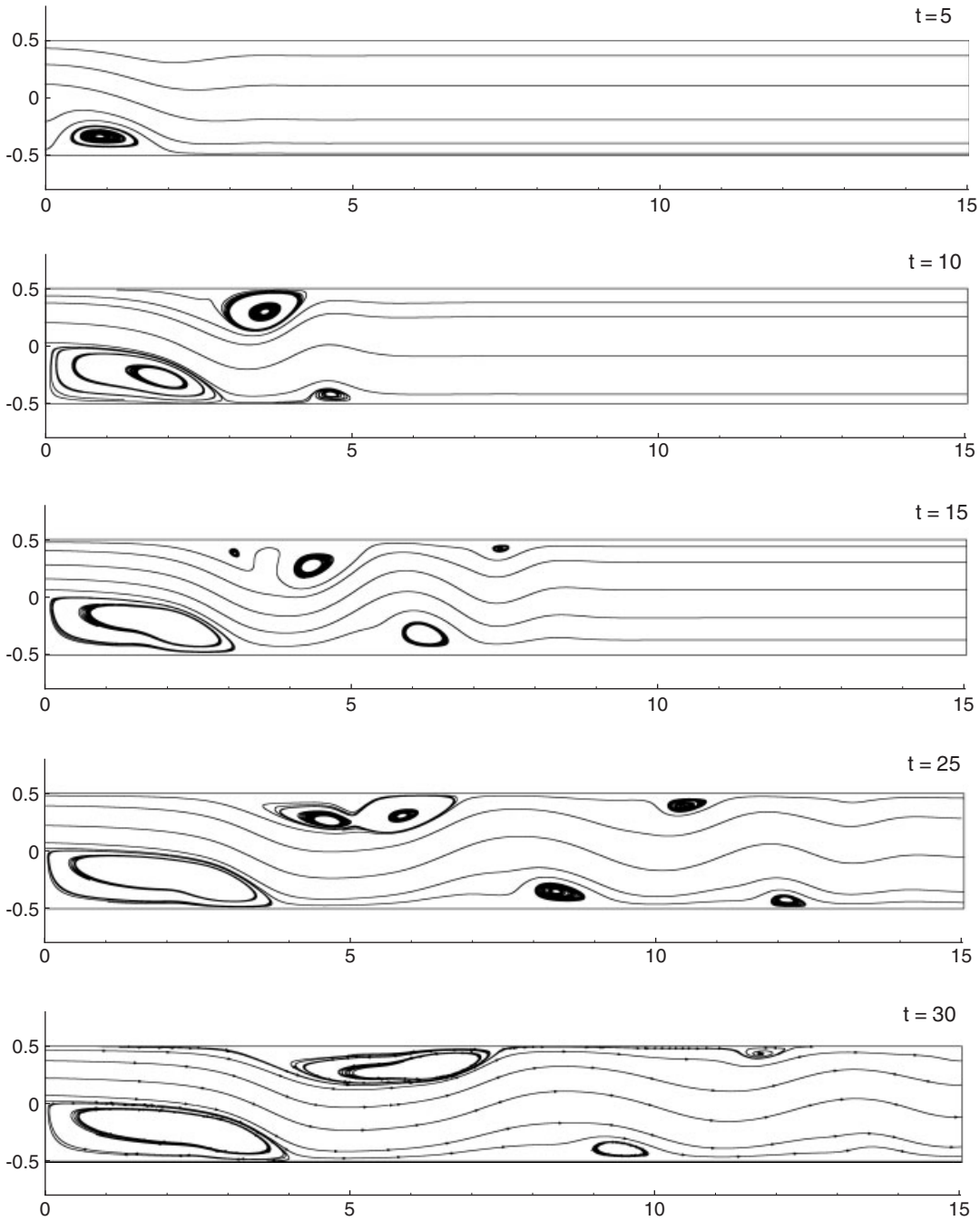

Figure 10. Time history of streamline plots for flow over a backward-facing step.

Copyright © 2008 John Wiley & Sons, Ltd.

DOI: 10.1002/fld

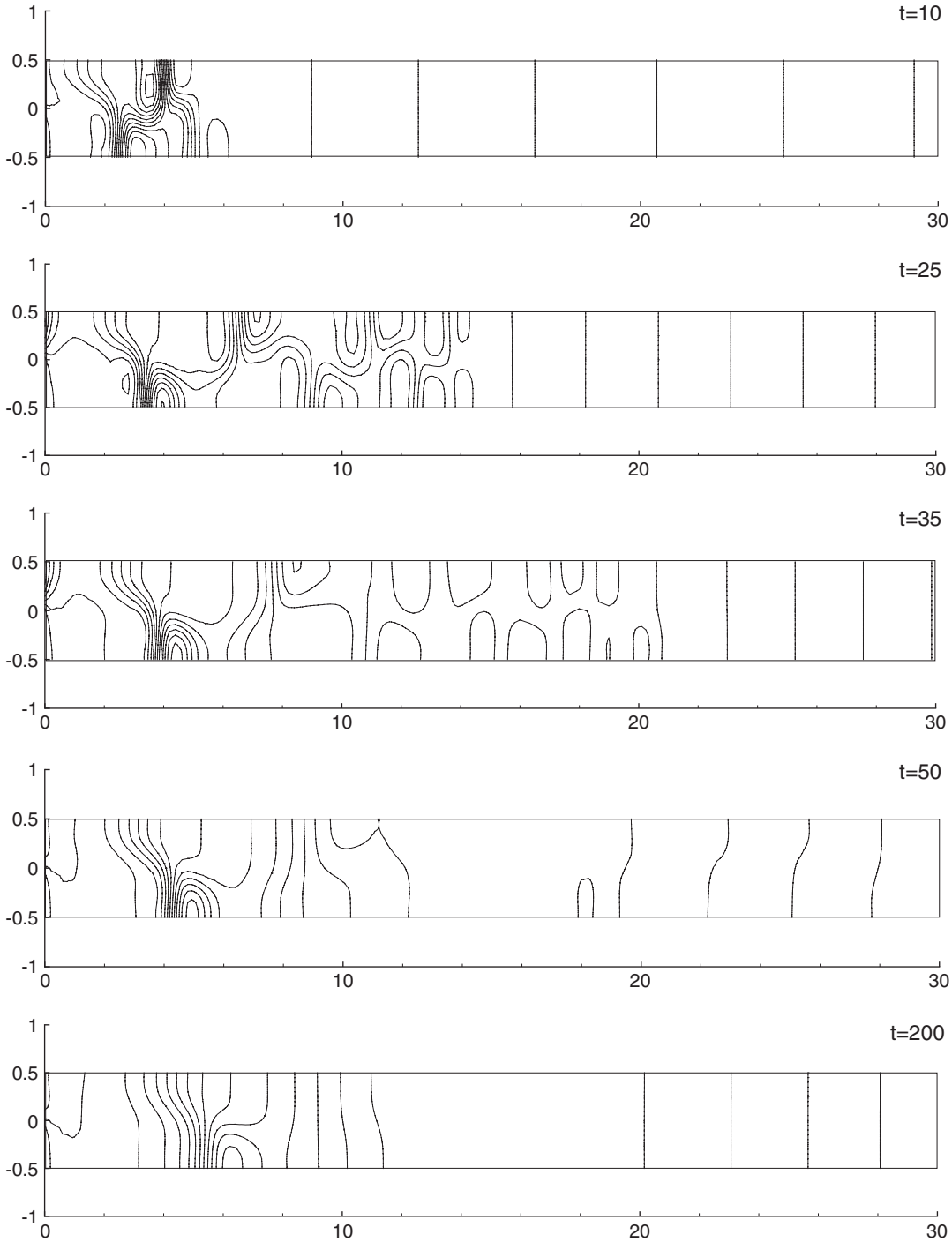

Figure 11. Time history of pressure contours for flow over a backward-facing step.

Copyright © 2008 John Wiley & Sons, Ltd.

DOI: 10.1002/fld

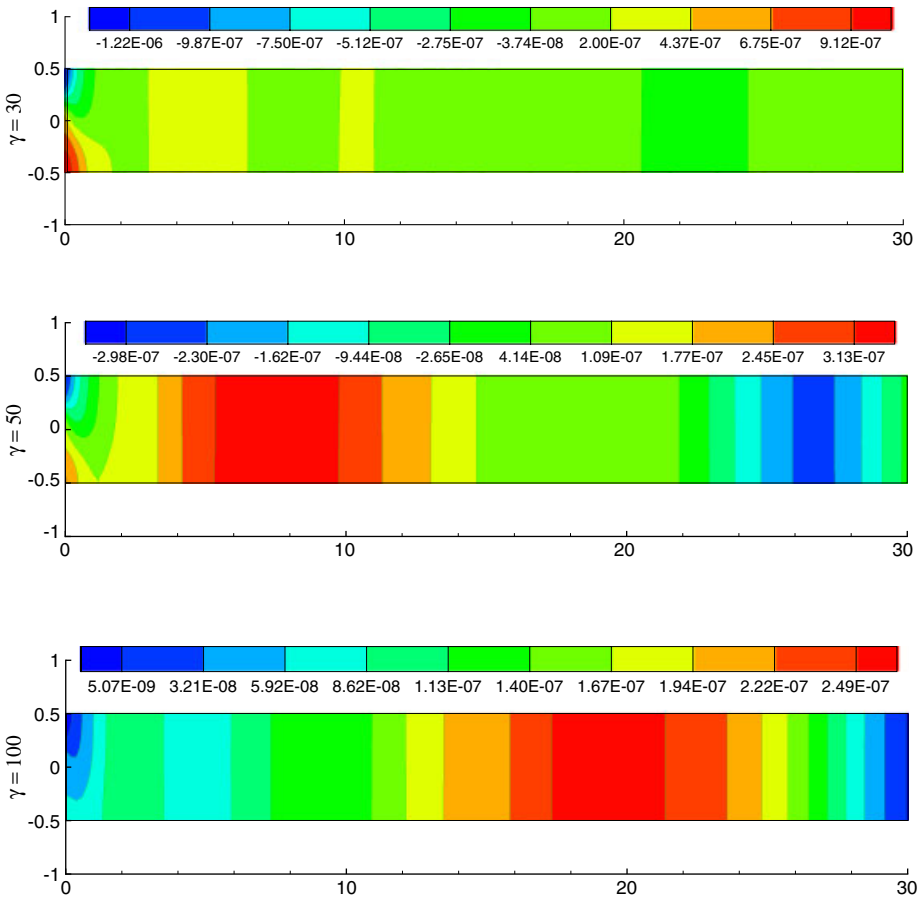

Figure 12. Dilatation contours at steady state for three penalty parameters.

the inflow boundary. Here, $u_b(y) = \max[0, 24y(0.5-y)]$ is the true inlet boundary condition and $u_p(y) = 3(0.5-y)(0.5+y)$ is the Poiseuille flow observed infinitely far downstream at steady state. The initial velocity field is set to $u = u_p(y)$ and $v = 0$ everywhere in the computational domain. The inlet condition is varied fast but smoothly from Poisuille flow to flow over a backward-facing step.

To accurately resolve primary and secondary circulation zones, a nonuniform mesh is used. We use seventh-order nodal expansion in each element (Mesh A). There are 19 604 degrees of freedom in the mesh. We condense out all interior degrees of freedom, resulting in 5780 interface degrees of freedom and a bandwidth of 268. Simulations are carried out for penalty parameters of 30, 50 and 100. This problem has been solved using both BDF2 and Crank–Nicholson time integration schemes. They predict equally accurate results. It has been observed that for this problem Crank–Nicholson-based discretization requires less conjugate gradient iterations to converge than BDF2-based discretization. A time increment of $\Delta t = 0.2$ has been used for all the results reported in this section.

Copyright © 2008 John Wiley & Sons, Ltd.

DOI: 10.1002/fld

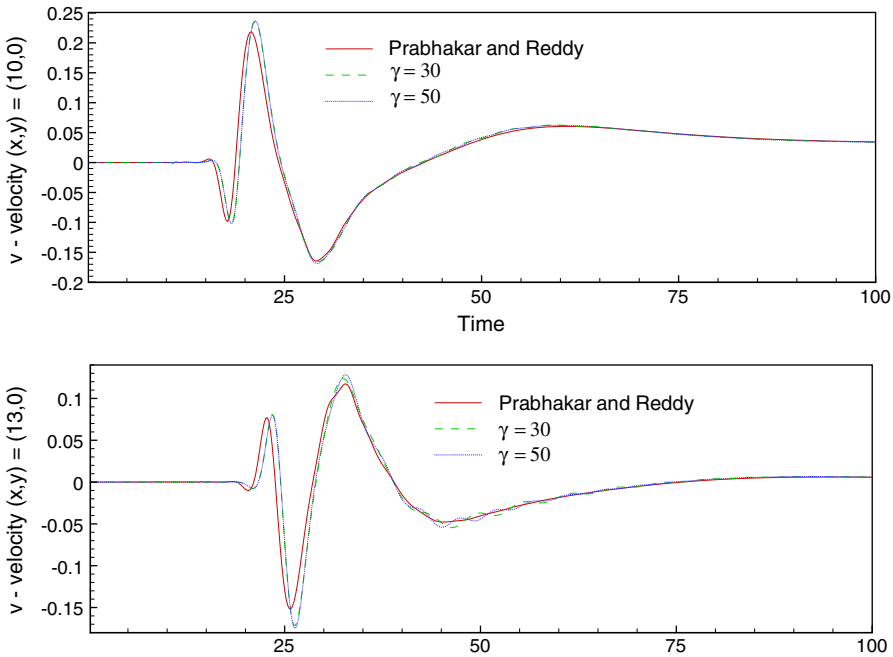

Figure 13. Time history of the v-velocity component at two selected locations: $P = 7$.

Figure 10 shows the evolution of the velocity flow field during initial stage. The main flow coming from the inlet follows a sinuous path, forming a series of eddies along the upper and lower walls. At steady state, two eddies (primary and secondary separation zones) remain, all other eddies die out. These plots match qualitatively well with the published results of Pontaza and Reddy [4] and Prabhakar *et al.* [9].

At steady state, the primary reattachment length is around 6.10, whereas the secondary separation and reattachment lengths are approximately 4.9 and 10.4, respectively. These values match very well with the published values of Gartling [18]. Figure 11 shows the evolution of pressure field. In this formulation, pressure field evolves smoothly. The pressure gradient caused by eddies can be seen in these plots. Dilatation contours at steady state are plotted in Figure 12 for three penalty parameters. The maximum value of the dilatation is around 10^{-6}, showing that mass conservation is very good.

The time history of v-velocity signal at two locations $(10, 0)$ and $(13, 0)$ is plotted in Figure 13 for penalty parameters of 30 and 50 and compared with the results of Prabhakar *et al.* [9], who used collocation penalty least-squares (bilinear shape functions with one-point Gauss quadrature). Results match well for both penalty parameters. For all the penalty parameters, we obtain smooth and monotonic decay of the transient. There are no fluctuations in the v-velocity field, showing that mesh resolution is adequate.

In Figures 14(a) and (b), the mass flow rate across sections $x = 5$ and 10 are plotted with time for penalty parameters of 30 and 50. There is less than 0.5% of mass loss for these penalty parameters, showing that mass conservation is very good even for low values of penalty parameters.

Copyright © 2008 John Wiley & Sons, Ltd.

DOI: 10.1002/fld

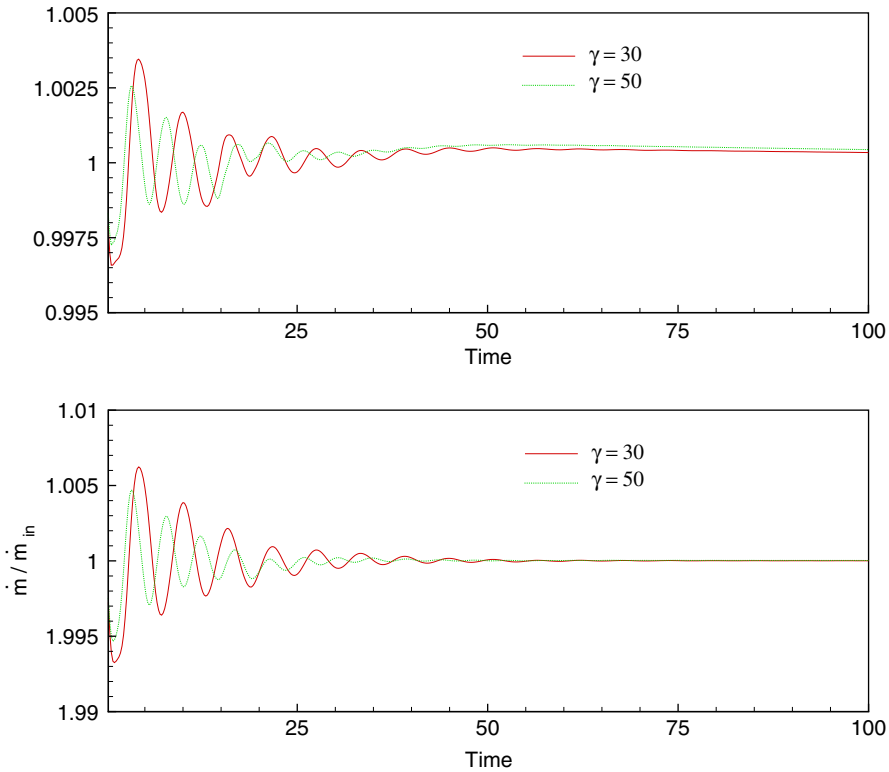

Figure 14. Time history of mass flow rate at (a) $x=5$ and (b) $x=10$; $P=7$.

Next, the number of PCG iterations required is plotted against time in Figure 15. The PCG solver converges steadily without much fluctuation (not shown here), indicating good conditioning of coefficient matrix. The penalty parameter is taken to be 30 in this case.

The previous works of Gresho *et al.* [17], Torczynski [19] and Pontaza and Reddy [4] showed that lack of spatial resolution induces unrealistic temporal chaotic behavior, resulting in an erroneous prediction of the long-term behavior of the flow. In such cases, either simulation diverges or the velocities fluctuate with time if it converges to steady state [4]. Pontaza and Reddy [4] reported that simulations diverge for p level less than 9 on 30×4 mesh, when space–time decoupled formulations are used. In our case, mesh is coarser than the one used in [4], but still simulations predict correct evolution of field and reach steady state. To examine sensitivity of accuracy on p-level, simulations are run for $p=5$ on 24×4 mesh (Mesh B) for penalty parameters of $30, 50$ and 100. Results are identical for penalty parameters of 50 and 100 (results for penalty parameter of 100 are not shown here). Time evolution of v-velocity at $(10, 0)$ is plotted in Figure 16 and compared with the results obtained using $p=7$ and $\gamma=50$ (reference curve). Even for p-level of 5, velocity evolution is quite accurate.

The L_2-norm of least-squares functional and dilatation are plotted in Figures 17(a) and (b) for p levels of 5 and 7 and a penalty parameter of 30. These plots show monotonic convergence to steady state.

Copyright © 2008 John Wiley & Sons, Ltd.

DOI: 10.1002/fld

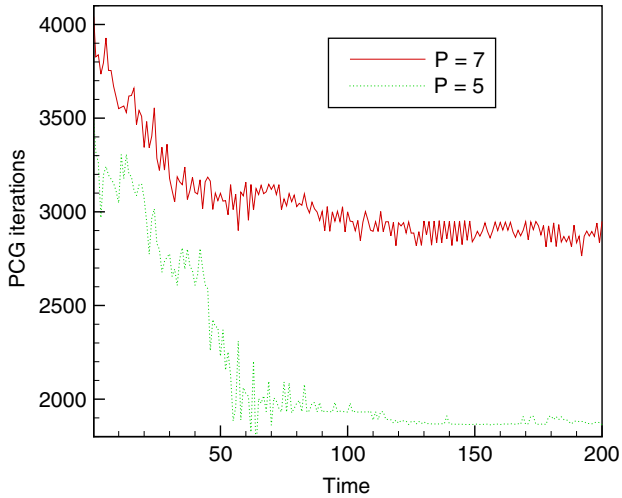

Figure 15. Time history of PCG iterations for flow over a backward-facing step.

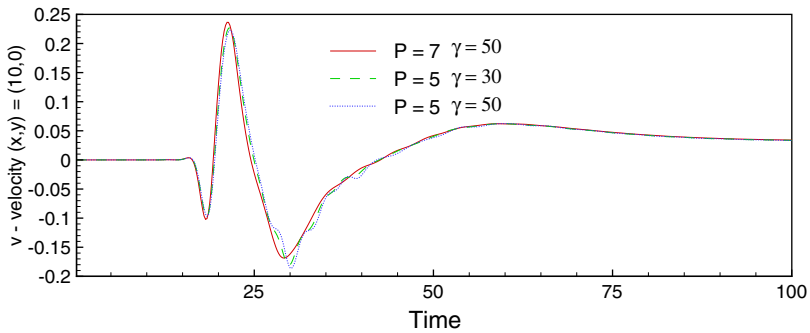

Figure 16. Time history of the v-velocity component at two selected locations: $P = 5$.

4. CONCLUDING REMARKS

In this paper, we presented a penalty least-squares finite element formulation for unsteady incompressible Navier–Stokes equations. The least-squares model was formed in terms of velocity, vorticity and dilatation. Space–time decoupled formulations were used for time discretization. Second-order accuracy of time integration scheme was verified using the method of manufactured solution. Numerical results were presented for impulsively started lid-driven cavity and flow over a backward-facing step problem. For these numerical examples, the effect of penalty parameter on the accuracy was investigated thoroughly and it was concluded that the present model produces accurate results even for low penalty parameters (10–50).

Copyright © 2008 John Wiley & Sons, Ltd.

DOI: 10.1002/fld

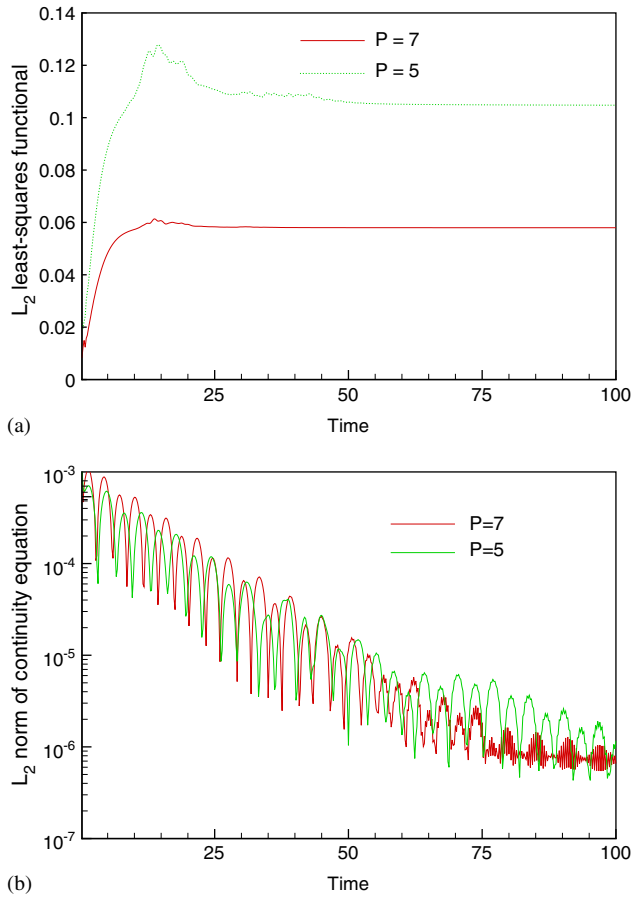

Figure 17. Time history of the (a) L_2 least-squares functional for $P=5$ and 7 and (b) L_2-norm of the continuity equation for $P=5$ and 7.

We presented this formulation as an alternative to traditional least-squares formulation, which has problems with pressure evolution. Pressure evolves smoothly in this formulation as verified through numerical examples. The present penalty least-squares finite element model is a better alternative to traditional penalty finite element model also. The advantage of the present model is that it gives very accurate results for very low penalty parameters. This formulation produces SPD coefficient matrix, whereas penalty finite element formulation produces unsymmetric indefinite coefficient matrix, which is computationally very expansive to solve.

ACKNOWLEDGEMENTS

The authors gratefully acknowledge the support of this work by the Computational Mathematics Program of the Air Force Office of Scientific Research through Grant F49620-03-1-0201 and Structural Dynamics Program of Army Research Office through Grant 45508-EG.

Copyright © 2008 John Wiley & Sons, Ltd.

REFERENCES

1. Jiang BN. *The Least-squares Finite Element Method* (1st edn). Springer: Berlin, 1998.
2. Jiang BN. On the least-squares method. *Computer Methods in Applied Mechanics and Engineering* 1998; **152**:239–257.
3. Pontaza JP, Reddy JN. Spectral/*hp* least-squares finite element formulation for the Navier–Stokes equations. *Journal of Computational Physics* 2003; **190**:523–549.
4. Pontaza JP, Reddy JN. Space–time coupled spectral/*hp* least-squares finite element formulation for the incompressible Navier–Stokes equations. *Journal of Computational Physics* 2004; **197**:418–459.
5. Bochev PV, Gunzburger MD. Finite element methods of least-squares type. *SIAM Review* 1998; **40**:789–837.
6. Prabhakar V, Reddy JN. Spectral/*hp* penalty least-squares finite element formulation for the steady incompressible Navier–Stokes equations. *Journal of Computational Physics* 2006; **215**:274–297.
7. Prabhakar V, Reddy JN. A stress based least-squares finite element formulation for the incompressible Navier–Stokes equations. *International Journal for Numerical Methods in Fluids* 2007; **54**:1369–1385.
8. Bell BC, Surana KS. A space–time coupled *p*-version least squares finite element formulation for unsteady two-dimensional Navier–Stokes equations. *International Journal for Numerical Methods in Engineering* 1996; **39**:2593–2618.
9. Prabhakar V, Pontaza JP, Reddy JN. A collocation penalty least-squares finite element formulation for incompressible flows. *Computer Methods in Applied Mechanics and Engineering* 2008; **197**:449–463.
10. Reddy JN. *An Introduction to the Finite Element Method* (3rd edn). McGraw-Hill: New York, 2006.
11. Reddy JN. *Introduction to Nonlinear Finite Element Analysis*. Oxford University Press: Oxford, 2004.
12. Reddy JN, Gartling DK. *The Finite Element Method in Heat Transfer and Fluid Dynamics* (2nd edn). CRC Press: Boca Raton, FL, 2001.
13. Gunzburger MD. Iterated penalty methods for the Stokes and Navier–Stokes equations. In *Finite Element Analysis in Fluids*, *Proceedings of the 7th International Conference on Finite Element Methods in Flow Problems*, Chung TJ, Karr GR (eds). University of Alabama Press: Alabama, 1989; 1040–1045.
14. Karniadakis GE, Sherwin SJ. *Spectral/hp Element Methods for CFD*. Oxford University Press: Oxford, 1999.
15. Salari K, Knupp P. *Verification of Computer Codes in Computational Science and Engineering*. Chapman & Hall/CRC Press: New York, 2003.
16. Ghia U, Ghia K, Shin CT. High-Re solutions for incompressible flow using the Navier–Stokes equations and a multigrid method. *Journal of Computational Physics* 1982; **48**:387–411.
17. Gresho PM, Gartling DK, Torczynski JR, Cliffe KA, Winters KH, Garrat TJ, Spence A, Goodrich JW. Is the steady viscous incompressible two-dimensional flow over a backward-facing step at Re = 800 stable? *International Journal for Numerical Methods in Fluids* 1993; **17**:501–541.
18. Gartling DK. A test problem for outflow boundary conditions—flow over a backward-facing step. *International Journal for Numerical Methods in Fluids* 1990; **11**:953–967.
19. Torczynski JR. A grid refinement study of two-dimensional transient flow over a backward-facing step using a spectral element method. In *Separated Flows*, vol. 149, Duuton JC, Purtell LP (eds). ASME: New York, 1993; 44–62.

Copyright © 2008 John Wiley & Sons, Ltd.

DOI: 10.1002/fld